JACS
JOURNAL OF THE AMERICAN CHEMICAL SOCIETY
Cite This: J. Am. Chem. Soc. 2018, 140, 6793−6796
Communication
pubs.acs.org/JACS

Atomic Force Microscopy Nanomechanical Mapping Visualizes Interfacial Broadening between Networks Due to Chemical Exchange Reactions

Changfei He,[†] Shaowei Shi,*[,†] Xuefei Wu,[†] Thomas P. Russell,*[,†,‡,§,∥] and Dong Wang*[,†]

[†]Beijing Advanced Innovation Center for Soft Matter Science and Engineering & State Key Laboratory of Organic−Inorganic Composites, Beijing University of Chemical Technology, Beijing 100029, China

[‡]Polymer Science and Engineering Department, University of Massachusetts, Amherst, Massachusetts 01003, United States

[§]Materials Sciences Division, Lawrence Berkeley National Laboratory, 1 Cyclotron Road, Berkeley, California 94720, United States

[∥]Advanced Institute for Materials Research, Tohoku University, 2-1-1 Katahira, Aoba, Sendai 980-8577, Japan

Supporting Information

ABSTRACT: The interfacial broadening between two different epoxy networks having different moduli was nanomechanically mapped. The interfacial broadening of the two networks produced an interfacial zone having a gradient in the concentration and, hence, properties of the original two networks. This interfacial broadening of the networks leads to the generation of a new network with a segmental composition corresponding to a mixture of the original two network segments. The intermixing of the two, by nature of the exchange reactions, was on the segmental level. By mapping the time dependence of the variation in the modulus at different temperatures, the kinetics of the exchange reaction was measured and, by varying the temperature, the activation energy of the exchange reaction was determined.

Vitrimers, polymer networks that can reconfigure by activated associative bond-exchange reactions of the junction points, are dynamic, and the network can respond to externally applied forces, redistribute the cross-link points, relieving any stresses, and remain virtually unchanged. These materials combine the ability to be reshaped, like a thermoplastic, with the permanent set characteristic of a cross-linked network.[1] At service temperature, vitrimers behave like thermosets (permanently cross-linked polymers) and exhibit high strength, good structural stability, and solvent resistance.[2] When they are heated, by exposure to light or other stimulus that activates the bonding dynamics, the junction points undergo reversible exchange reactions, allowing the network break but then reform due to the reversible exchange reactions. Subsequent to the pioneering work of Leibler and co-workers,[3] a series of vitrimers have been produced by different types of dynamic covalent bonding reactions, e.g. transesterification,[4−10] transamination,[11−14] imine amine exchange reaction,[15−18] transcarbamoylation,[19,20] disulfide exchange reaction,[21−24] olefin metathesis exchange reaction,[25] and alkoxysilane exchange reaction.[26−28] These materials have obvious advantages as recyclable or self-healing materials. Such dynamic covalent bonding can, also, be used to promote adhesion between two immiscible polymers,[2] where local exchange reactions can serve to broaden an interface, effectively chemically bonding one material to another.

It is, of course, impossible for two conventional networks to undergo interdiffusion due to the network structure. With vitrimers, though, the dynamic covalent bonding allows the cross-links to be broken and reformed such that, when the cross-links are broken, segmental exchange can occur, and upon reformation of the cross-links, a gradient in the chemical composition of the networks at the interface will result whereby, over extended or repeated thermal cycling, long-range interfacial broadening can be realized. Ultimately, a single new network would be produced with a random spatial distribution of the different segments with properties intermediate between the two original networks. If the moduli of the networks are different, then the segmental mixing of the two networks can be tracked by atomic force microscopy nanomechanical mapping (AFM-NM), by which information related to the local microstructure and mechanical properties can be provided simultaneously.[29−33] In the present work, we use a widely used AFM-NM in recent years, PeakForce QNM (Quantitative NanoMechanics) mode,[34−37] to monitor mechanical properties changes accompanying the chemical exchange reactions of two network polymers. The change in the properties can be used to determine local changes in the composition and, hence, the interchange reactions between the two networks and the interfacial broadening. By mapping the time dependence of the variation in the modulus at different temperatures, we determined the kinetics of the exchange reaction and, by varying the annealing temperature, the activation energy of the exchange reaction.

Epoxy networks having a high modulus (V1) and a low modulus (V2) were prepared by the classic reactions shown in Scheme S1 (Supporting Information (SI)). The storage modulus E' at glass stage for V1 is 2.15 GPa, while that for V2 is 195 MPa (Figure S1). This difference is more than sufficient to distinguish the two networks by AFM-NM. The thermal and thermomechanical properties of V1 and V2 are shown in Table S1. Stress−relaxation experiments showed that

Received: April 13, 2018
Published: May 18, 2018

DOI: 10.1021/jacs.8b03771
J. Am. Chem. Soc. 2018, 140, 6793−6796

the networks were fully relaxed at elevated temperatures, due to the transesterification reaction (Figure S3). The activation energies for V1 and V2 were calcluated to be 111 ± 2.5 and 98.4 ± 5 kJ/mol, respectively (SI, Note 2). The similarity of these energies indicates that the exchange reaction between V1 and V2 should be similar to that of V1 with V1 and V2 with V2; i.e., the inter- and intramolecular exchange should be the same. The topology freezing transition temperature, T_v,[3] for V1 and V2 were calculated be 37.4 and 13 °C (SI, Note 2), which is below their T_g of 47 and 25 °C, respectively. So in this system, when these two vitrimers are heated, their viscosities are initially controlled by diffusion (WLF) and then by the exchange reaction kinetics (Arrhenius).[1]

A series of networks with different mole fractions of curing agents were prepared, and these materials can be considered as mixtures of different ratios of V1 and V2 when they have segment exchange at the interface. DSC results show $1/T_g$ of network mixtures have a linear relationship with the composition of V1 (Figure S4), which agrees with the Fox equation, allowing us to determine the composition from the modulus in the AFM-NM studies. The Young's modulus obtained from tensile testing or AFM-NM show a linear relationship with the composition of V1 (Figure S5), indicating the modulus map can be converted into the concentration map. As expected, all these networks swelled and did not dissolve in the chlorobenzene at 120 °C and they all show similar gel fractions (Table S2).

Figure 1a shows a scheme of the bilayer sample and AFM-NM investigation on the interfacial broadening of the network bilayers. The purple area indicates V1 while the red area indicates V2. The Young's modulus (E) for V1 and V2, shown in the modulus profile, are 2.7 ± 0.15 GPa and 1.6 ± 0.2 GPa, respectively. The measured Young's modulus of V1 agrees with the bulk value of 2.8 ± 0.26 GPa, while the modulus of V2 is

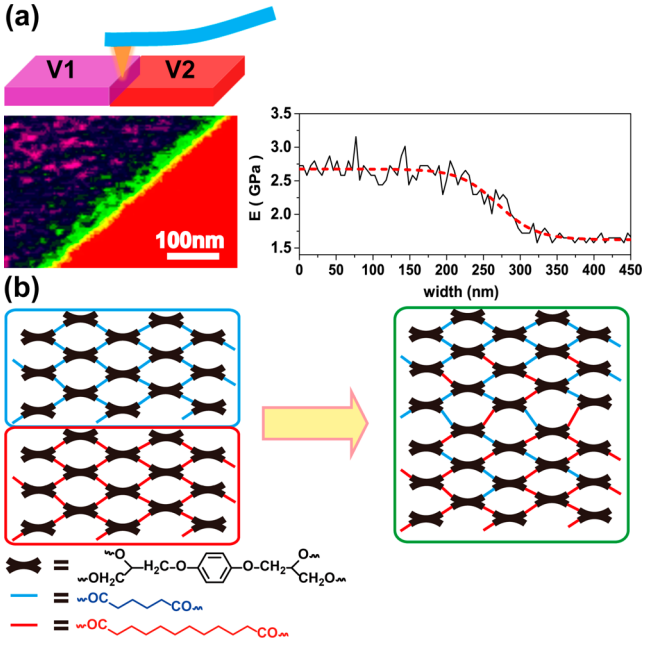

Figure 1. (a) Scheme of the vitrimer bilayer sample using AFM-NM and the 2D (colorized) Young's modulus mapping across the interface after thermal annealing for 40 min at 170 °C and the corresponding modulus profile across the interface (right). (b) Scheme of the interfacial broadening process of V1 and V2 networks.

several times higher than that of the bulk value of 0.2 ± 0.04 GPa, as measured by tensile testing (Figure S5). The modulus difference between AFM-NM and bulk measurements can be attributed to a higher speed of sample deformation (18 mm/min) by tip oscillation than that of the tensile testing (10 mm/min), which could yield an elastic modulus higher than that of bulk, especially for the soft materials. The second reason may come from the Young's modulus calculation (SI, Note 3). Young's modulus obtained both by AFM-NM and tensile testing show the same trend (linear relationship) with the chemical composition, as discussed previously. So, in this experiment, the modulus distribution can be used as a measure of the chemical compositions of V1 and V2.

A gradient region with colors changing from green to yellow is seen in Figure 1a, indicating that the modulus gradually decreases from the modulus of V1 to the modulus of V2, which is clear evidence of the interfacial broadening between V1 and V2. As shown schematically in Figure 1b, when V1 and V2 are in contact at a sufficiently high temperature, the hydroxyl groups can react with the ester groups in the presence of the catalyst. Under that condition, cross-link points continually break and reform, allowing the movement of V1 segments into the network of V2 and vice versa. Once V1 segments have exchanged with V2 segments, the modulus will change locally. As the exchange reaction continues, a gradient develops in the concentration and modulus across the interface (yet the bilayer is fully cross-linked).

A series of modulus maps across the interfacial regions and their corresponding profiles are shown in Figure 2, from short

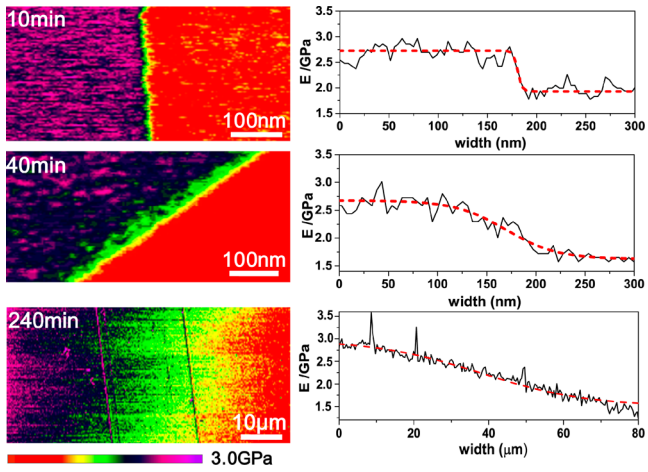

Figure 2. Young's modulus maps across the V1/V2 interface at 170 °C for different times and the corresponding modulus profiles. The red dash lines hyperbolic tangent function fit to the modulus data.

to extended annealing times at 170 °C. From the modulus map, we can see the transition region broadens from a sharp interface to hundreds of nanometers to many microns with increasing time. The width of the transition region was measured using the red dashedline that is the best-fit hyperbolic tangent function (determined using more than 20 single modulus profiles). The transition region consists of a new random network with segments of V1 and V2, where the chemistries of the cross-links are the same. The interfacial broadening process of the different vitrimers is very different from the interdiffusion of linear polymers.[35] For linear polymers, polymer chains interdiffuse, leading to formation of a transition region

DOI: 10.1021/jacs.8b03771
J. Am. Chem. Soc. 2018, 140, 6793−6796

consisting of two original polymer chains while, for vitrimer networks, segmental motions occur by segment exchange processes where a reversible chemical reaction occurs between each step leading to the formation of a new network consisting of segments that comes from each vitrimer. The exchange reaction can occur in the forward and reverse direction, though entropy favors the mixing of the different segments. Since both vitrimer networks have alkyl chains, the enthalpy contribution should be small. Consequently, with increasing time the interface will broaden where the time dependence is governed by the activation energy of the transesterification reaction.

The modulus profile can be converted to a concentration profile based on a linear relationship between the Young's modulus (E) and vitrimer composition (Figure S6). From the concentration profile, we define the relationship between the transition region width w and the transesterification rate k. The k is determined from eq 1 (more details in the SI, Note 4),

$$\ln\left(\frac{w}{w_0}\right) = kt \tag{1}$$

where w is the transition region width and w_0 is the initial width that is determined by average transition width at 10 min. w_0 is calculated to be 11.9 ± 1.1 nm, independent of the temperature. Figure 3 shows the exchange reaction rate varies

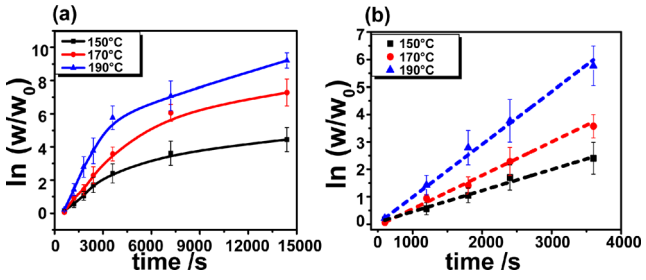

Figure 3. (a) $\ln(w/w_0)$ as a function of annealing time at 150, 170, and 190 °C. (b) $\ln(w/w_0)$ as a function of time from 600 to 3600 s.

with time. The interfacial broadening of V1 and V2 (segments exchange process) exhibits three distinct stages. For times less than 10 min, driven by entropy, unattached and dangling chains in the network will diffuse and reach equilibrium in a very short annealing time. All bilayers had an interfacial width of ~10 nm due to the mobility of unattached and dangling chains. During this short time, there is almost no segment exchange and the exchange rate is nearly 0. While in the second stage, from 10 to 60 min, the exchange reaction begins to occur and we find the exchange reaction rate increases linearly with time as seen in Figure 3b, which agrees with a first-order transesterification reaction. The values of k determined from the initial slope of the fitting lines at annealing temperatures of 150, 170, and 190 °C are $(7.73 \pm 0.62) \times 10^{-4}$, $(1.16 \pm 0.05) \times 10^{-3}$, and $(1.83 \pm 0.09) \times 10^{-3}$ s^{-1} respectively. k is temperature dependent; it will increase with increasing temperature. After the rapid increase in the width of the transition region, in the third stage, the broadening slows as the number of intermolecular exchanges decrease due to the equilibrium of the reversible exchange reaction.

The width of the transition region is observed to increase with temperature in Figure S6. The k varies with temperature and follows the Arrhenius equation, allowing us to calculate the exchange activation energy of the epoxy system. From a plot of $\ln(w/w_0)$ as a function of $1/T$ (Figure 4), the slope of the straight line yields an activation energy E_a = 93.6 ± 6.3 kJ/mol.

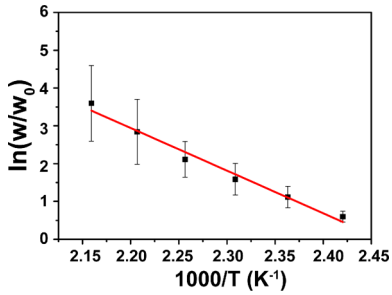

Figure 4. $\ln(w/w_0)$ as a function of $1/T$ at 40 min. Slope yields an apparent activation energy for exchange of 93.6 kJ/mol for the epoxy system.

This activation energy is very similar to the value of 88 kJ/mol, reported by Leibler and co-workers for the activation energy of an epoxy vitrimer.[3] These values also correspond to the value determined by stress–relaxation, opening a new route to estimate the barrier energy of vitrimer networks.

In summary, a novel way to monitor the exchange reaction across the interface of two different solid networks by using AFM nanomechanical mapping was shown where segment exchange resulted in a detectable modulus and composition variation across the interface. We found the interfacial broadening process was markedly different from that of linear polymers, as would be expected. The interfacial rearrangements of the two vitrimer networks occurred in a stepwise manner with the interfacial broadening following a first-order reaction rate behavior. The activation energy was calculated from the temperature dependence of the width of the interface at a specific time, which was found to agree with that obtained from the stress–relaxation measurements. The protocols open a new pathway to estimate the barrier energy of vitrimer networks.

■ ASSOCIATED CONTENT

Supporting Information

The Supporting Information is available free of charge on the ACS Publications website at DOI: 10.1021/jacs.8b03771.

Experimental details and characterization data (PDF)

■ AUTHOR INFORMATION

Corresponding Authors

*shisw@mail.buct.edu.cn
*russell@mail.pse.umass.edu
*dwang@mail.buct.edu.cn

ORCID

Shaowei Shi: 0000-0002-9869-4340
Thomas P. Russell: 0000-0001-6384-5826
Dong Wang: 0000-0003-2326-0852

Notes

The authors declare no competing financial interest.

■ ACKNOWLEDGMENTS

This work was supported by National Natural Science Foundation of China (51673016).

DOI: 10.1021/jacs.8b03771
J. Am. Chem. Soc. 2018, 140, 6793–6796

REFERENCES

(1) Kloxin, C. J.; Bowman, C. N. *Chem. Soc. Rev.* **2013**, *42*, 7161−7173.
(2) Rottger, M.; Domenech, T.; van der Weegen, R.; Breuillac, A.; Nicolay, R.; Leibler, L. *Science* **2017**, *356*, 62−65.
(3) Montarnal, D.; Capelot, M.; Tournilhac, F.; Leibler, L. *Science* **2011**, *334*, 965−968.
(4) Capelot, M.; Montarnal, D.; Tournilhac, F.; Leibler, L. *J. Am. Chem. Soc.* **2012**, *134*, 7664−7667.
(5) Altuna, F. I.; Pettarin, V.; Williams, R. J. J. *Green Chem.* **2013**, *15*, 3360−3366.
(6) Brutman, J. P.; Delgado, P. A.; Hillmyer, M. A. *ACS Macro Lett.* **2014**, *3*, 607−610.
(7) Pei, Z.; Yang, Y.; Chen, Q.; Terentjev, E. M.; Wei, Y.; Ji, Y. *Nat. Mater.* **2014**, *13*, 36−41.
(8) Yang, Y.; Pei, Z.; Li, Z.; Wei, Y.; Ji, Y. *J. Am. Chem. Soc.* **2016**, *138*, 2118−2121.
(9) Cromwell, R.; Chung, J.; Guan, Z. *J. Am. Chem. Soc.* **2015**, *137*, 6492−6495.
(10) Legrand, A.; Soulié-Ziakovic, C. *Macromolecules* **2016**, *49*, 5893−5902.
(11) Fortman, D. J.; Brutman, J. P.; Cramer, C. J.; Hillmyer, M. A.; Dichtel, W. R. *J. Am. Chem. Soc.* **2015**, *137*, 14019−14022.
(12) Denissen, W.; Rivero, G.; Nicolaÿ, R.; Leibler, L.; Winne, J. M.; Du Prez, F. E. *Adv. Funct. Mater.* **2015**, *25*, 2451−2457.
(13) Ying, H.; Zhang, Y.; Cheng, J. *Nat. Commun.* **2014**, *5*, 3218.
(14) Denissen, W.; Droesbeke, M.; Nicolay, R.; Leibler, L.; Winne, J. M.; Du Prez, F. E. *Nat. Commun.* **2017**, *8*, 14857.
(15) Taynton, P.; Yu, K.; Shoemaker, R. K.; Jin, Y.; Qi, H. J.; Zhang, W. *Adv. Mater.* **2014**, *26*, 3938−3942.
(16) Lei, Z. Q.; Xie, P.; Rong, M. Z.; Zhang, M. Q. *J. Mater. Chem. A* **2015**, *3*, 19662−19668.
(17) Chao, A.; Negulescu, I.; Zhang, D. *Macromolecules* **2016**, *49*, 6277−6284.
(18) Taynton, P.; Ni, H.; Zhu, C.; Yu, K.; Loob, S.; Jin, Y.; Qi, H. J.; Zhang, W. *Adv. Mater.* **2016**, *49*, 6277−6284.
(19) Zheng, N.; Fang, Z.; Zou, W.; Zhao, Q.; Xie, T. *Angew. Chem., Int. Ed.* **2016**, *55*, 1−6.
(20) Zheng, N.; Hou, J.; Xu, Y.; Fang, Z.; Zou, W.; Zhao, Q.; Xie, T. *ACS Macro Lett.* **2017**, *6*, 326−330.
(21) Michal, B. T.; Jaye, C. A.; Spencer, E. J.; Rowan, S. J. *ACS Macro Lett.* **2013**, *2*, 694−699.
(22) Pepels, M.; Filot, I.; Klumperman, B.; Goossens, H. *Polym. Chem.* **2013**, *4*, 4955−4965.
(23) Lei, Z. Q.; Xiang, H. P.; Yuan, Y. J.; Rong, M. Z.; Zhang, M. Q. *Chem. Mater.* **2014**, *26*, 2038−2046.
(24) Wei, C.; Chen, M.; Liu, D.; Zhou, W.; Khan, M.; Wu, X.; Huang, N.; Li, L. *Polym. Chem.* **2015**, *6*, 4067−4070.
(25) Capelot, M.; Montarnal, D.; Tournilhac, F.; Leibler, L. *J. Am. Chem. Soc.* **2012**, *134*, 7664−7667.
(26) Osthoff, R. C.; Bueche, A. M.; Grubb, W. T. *J. Am. Chem. Soc.* **1954**, *76*, 4659−4663.
(27) Zheng, P.; McCarthy, T. J. *J. Am. Chem. Soc.* **2012**, *134*, 2024−2027.
(28) Nishimura, Y.; Chung, J.; Muradyan, H.; Guan, Z. *J. Am. Chem. Soc.* **2017**, *139*, 14881−14884.
(29) Sahin, O.; Magonov, S.; Su, C. M.; Quate, C. F.; Solgaard, O. *Nat. Nanotechnol.* **2007**, *2*, 507−514.
(30) Jesse, S.; Kalinin, S. V.; Proksch, R.; Baddorf, A. P.; Rodriguez, B. J. *Nanotechnology* **2007**, *18*, 435503.
(31) Stan, G.; Cook, R. F. *Nanotechnology* **2008**, *19*, 235701.
(32) Garcia, R.; Herruzo, E. T. *Nat. Nanotechnol.* **2012**, *7*, 217−226.
(33) Garcia, R.; Proksch, R. *Eur. Polym. J.* **2013**, *49*, 1897−1906.
(34) Wang, D.; Nakajima, K.; Liu, F.; Shi, S.; Russell, T. P. *ACS Nano* **2017**, *11*, 8660−8667.
(35) Wang, D.; Russell, T. P.; Nishi, T.; Nakajima, K. *ACS Macro Lett.* **2013**, *2*, 757−760.
(36) Sokolova, M. P.; Smirnov, M. A.; Bugrov, A. N.; Geydt, P.; Popova, E. N.; Lahderanta, E.; Svetlichnyi, V. M.; Toikka, A. M. *Polymers* **2017**, *9*, 268.
(37) Smolyakov, G.; Pruvost, S.; Cardoso, L.; Alonso, B.; Belamie, E.; Duchet-Rumeau, J. *Carbohydr. Polym.* **2016**, *151*, 373−380.

DOI: 10.1021/jacs.8b03771
J. Am. Chem. Soc. 2018, 140, 6793−6796